PERGAMON

European Journal of Cancer 38 (2002) 2173–2188

European Journal of Cancer

www.ejconline.com

Small animal imaging: current technology and perspectives for oncological imaging

Jason S. Lewis[a,d], S. Achilefu[b,d], J.R. Garbow[c,d], R. Laforest[a,d], M.J. Welch[c,d,*]

[a]*Radiation Sciences, Washington University School of Medicine, Saint Louis, MO, USA*
[b]*Optical Radiology Laboratory, Washington University School of Medicine, Saint Louis, MO, USA*
[c]*Biomedical MR Laboratory, Mallinckrodt Institute of Radiology, Washington University School of Medicine, Saint Louis, MO, USA*
[d]*Alvin J. Siteman Cancer Center, Washington University School of Medicine, Saint Louis, MO, USA*

Received 31 May 2002; accepted 1 August 2002

Abstract

Advances in the biomedical sciences have been accelerated by the introduction of many new imaging technologies in recent years. With animal models widely used in the basic and pre-clinical sciences, finding ways to conduct animal experimants more accurately and efficiently becomes a key factor in the sucess and timeliness of research. Non-invasive imaging technologies prove to be extremely valuable tools in performing such studies and have created the recent surge in small animal imaging. This review is focused on three modalities, PET, MR and optical imaging which are avaliable to the scientist for oncological investigations in animals.

Keywords: Small animal imaging; PET; MRI; Optical; Transgenic

1. Introduction

Advances in the biomedical sciences have been accelerated by the introduction of many new imaging technologies in recent years. With animal models widely used in the basic and preclinical sciences, finding ways to conduct animal experiments more accurately and efficiently becomes a key factor in the success and timeliness of research. Recent revolutions in molecular biology and genomics have created a large demand for transgenic laboratory animals. The most efficient way of establishing such models is through longitudinal studies on laboratory animals over an extended period of time. Non-invasive imaging technologies prove to be extremely valuable tools in performing such studies and have created the recent surge in small animal imaging [1].

The new transgenic cancer models are expensive and often exhibit sporadic development of tumours. These tumours are often located in remote sites that preclude measurement by traditional palpation. It is therefore difficult to establish whether cancer is present prior to experimental therapies. Utilisation of these models relies on autopsy and histology to determine whether the cancer has developed. The small animal imaging tools now available would enable prescreening of animals to ensure the presence of cancer in these transgenic models prior to therapy. At the beginning of the treatment phase of studies (following tumour induction), imaging could be used to phenotype mice for similar tumour loads. Then, after treatment, tumour response to treatment over time can be monitored. The use of imaging modalities to non-invasively study various disease states has been reviewed and the reader is directed to two extensive articles that have recently appeared [1,2]. The article by Budinger and colleagues discusses multiple aspects of imaging transgenic mice and how different imaging modalities can be applied [1], the article by Weissleder presents an interesting comparison between each technique including an overview of each modality, resolutions, uses and costs [2].

2. CT, SPECT and ultrasound imaging

Although this review is focused on the imaging modalities available to the scientist for oncological investigations in animals, three modalities, Positron Emission

* Corresponding author. Tel.: +314-362-8435; fax: +314-362-8399.
E-mail address: welchm@mir.wustl.edu (M.J. Welch).

0959-8049/02/$ - see front matter
PII: S0959-8049(02)00394-5

Tomography (PET), Magnetic Resonance (MR) and Optical Imaging are to be focused on. Magnetic Resonance Imaging (MRI) imaging is so well established that a full review would be so extensive that it does not fall within the scope of this article, therefore only a brief summary is presented. Three other important modalities, single photon emission computed tomography (SPECT), X-ray computed tomography (CT) and ultrasound also require a brief mention. For these modalities, the reader is directly to a number of excellent reviews.

A dedicated animal CT scanner (microCT) is capable of providing high-resolution (50 μm) three-dimensional anatomical images of small laboratory animals such as mice and rats. Such systems have been primarily used for bone imaging applications [3–5], due to the favourable contrast between bone mineral and soft tissues. High-resolution microCT systems have also been shown to be effective in soft-tissue tumour imaging e.g. [6], and phenotyping of disease in transgenic models [7]. MicroCT offers the opportunity to perform high-throughput imaging of large numbers of transgenic models to phenotype a disease state due to its fast imaging times and high spatial resolutions [7,8]. With the use of iodinated contrast agents, the image contrast can be significantly improved. A series of recent reviews have discussed the design issues and technology behind the microCT systems and potential applications [3,8,9].

SPECT imaging requires a gamma camera capable of imaging the subject injected with a labelled radiopharmaceutical. The gamma-emitting radionuclide of choice should decay with the emission of a low-energy gamma in order to improve counting rate capability and image resolution. In SPECT mode, the camera rotates around the subject, or the animal, in order to acquire a complete set of tomographic projections. SPECT systems with either pinhole collimators [10,11] or parallel-hole collimators [12] have been developed for use in small-animal laboratories [13–15] with spatial resolutions as high as 1–2 mm. These systems take advantage of the large number of gamma-emitting radiopharmaceuticals (small molecule, peptide and antibody probes) that are either routinely used in the clinic or are under development.

Ultrasound imaging can have a resolution as high as 50 μm since the generated images are based on acoustic echoes resulting from high-frequency acoustic waves. It is relatively cheap, inexpensive and portable, but is limited to the depth of tissue that can be scanned though, and image quality can be affected by the presence of artifacts caused by the existence of bone or air. As a consequence, the use of ultrasound in animal imaging has not been as extensive as other modalities and has instead focused upon delineating accessible biological entities such as bladder tumours [16] and blood flow [17].

3. MR imaging

MRI is a powerful and versatile imaging modality for animal studies. Most MRI experiments involve visualising water, which is ubiquitous in animal tissues and organs. Water has a wide variety of biophysical magnetic signatures in tissues and organs and a key to success in many experiments is optimising experimental methods and parameters to enhance contrast between healthy and diseased tissue. Over the last decade, MRI has been used extensively in the characterisation of tumours in a wide variety of animal models. Monitoring *in vivo* tumour growth and ablation in response to therapy is, perhaps, the most straightforward application of MRI in the study of cancer. Here, the non-invasive, non-destructive nature of MRI is particularly advantageous, as one can serially monitor individual subjects of a given cohort over an extended time period. However, MRI methods are also being developed and applied to address many other important issues in oncology, including: (1) early detection of precancerous tissue before tumours are visible; (2) detailed characterisation of cancerous tissue—What are the unique properties of this tissue and do these properties provide insights that suggest potential treatments?; (3) characterisation of angiogenesis and the role of the developing vasculature in tumour growth and development; (4) elucidation of mechanisms and processes by which *in situ* carcinoma evolves into invasive carcinoma—since cancer mortality is principally associated with the consequences of tumour invasion and dissemination, such an understanding will have major therapeutic implications.

One of MRI's major roles has been in helping to develop and validate new animal models of cancer, in part by accurately measuring the growth of tumours in longitudinal animal studies. MRI has recently been applied to the development of animal models of cancer in brain [18–20], lung [21], kidney [22], bladder [23], prostate [24] and pancreas [25], as well as primary central nervous system lymphoma [26]. MRI has also been used to monitor the effects of cancer therapy in a wide variety of animal tumour models. Recent applications include studies of chemotherapeutic treatment of models of brain [27,28], prostate [29], colon [30], bladder [31], and liver [32] cancer, the development of tumours at wound sites following laparoscopic surgery [33] as well as responses to gene therapy in models of glioma [34,35]. As described above, one of the major challenges in MRI is the optimisation of experimental conditions to enhance the contrast between healthy and diseased tissue. In oncology, the goal of early detection of cancerous tissue has fuelled the active development and use of contrast agents to aid in the visualisation of tumours. (One of the great strengths of MRI is that there exists a myriad of biophysical magnetic-related phenomena through which one can generate tissue contrast.) In many cases, these agents have been developed to target tumours in specific organs. Applications in the study of

animal models of brain [36–38], breast [39], liver [40], ovarian [41], and lymph node [42] cancers, as well as melanoma [43,44] and squamous-cell carcinoma [45] have recently been described.

As previously noted, much cancer research has focused on understanding the conditions that promote tumour metastasis and/or proliferation and numerous MRI studies have aimed at providing insights into tumour viability and growth [46–48]. Angiogenesis, the formation of new blood vessels, an important step in the growth of many tumours, is an extremely active area of oncological research. A more fundamental understanding of the role of angiogenesis will provide important insights into tumour growth and progression and may lead to the development of anti-angiogenesis drugs for cancer treatment. Interest in the tumour vasculature has driven the development of dynamic contrast enhanced (DCE) MRI as a marker of angiogenesis and for measuring fractional blood volume and microvascular permeability, and applications of the blood oxygen level dependent (BOLD) effect for assessing blood oxygenation. In the basic DCE experiment, a series of highly time-resolved (seconds) images are collected before, during and after the injection of contrast agent and the observed time-dependent intensity changes are modelled to derive parameters describing the tumour vasculature (e.g. flow, volume, permeability). These experiments have been applied to a wide variety of tumour systems to provide insight into vascular development [49–51] and have been used to assess the effects of new drugs and therapies on tumours [52,53]. Recently, significant effort has been devoted to the development of new macromolecular contrast agents that can help to provide more direct, specific information about tumour vasculature [54–56]. Blood flow and tumour oxygenation can significantly affect response to chemotherapy and radiation. BOLD MRI has been used to measure tumour blood flow and oxygenation under a variety of different conditions (e.g. carbogen (95% oxygen, 5% carbon dioxide) breathing, presence of tumour-oxygenating agents) relevant to tumour therapy [57–60].

In summary, MR is a powerful, versatile imaging modality for oncology studies. The high spatial resolution of MR images permits the growth and development of tumours to be accurately measured. A wide range of different experimental conditions and chemical agents can be used to enhance contrast in these images. Its sensitivity to dynamic processes, including diffusion, perfusion and flow, make MR an excellent modality for studying the tumour vasculature and oxygenation.

4. PET imaging

Human PET imaging is used in the non-invasive diagnosis of medical problems such as cancer, infection, kidney and liver abnormalities, cardiological and neurological disorders. PET is unique because it produces images of the body's basic biochemistry or function. Traditional diagnostic techniques, such as X-rays, CT scans or MRI, produce images of the body's anatomy or structure. PET imaging uses radiolabelled tracers to reveal biological functions. With carefully designed labelled molecular probes, the target can be a specific metabolite, a tumour-specific antigen, or a gene being expressed. The functions being revealed could be a signal transduction in neurological systems, development of tumour under controlled environments, or the mechanism of a gene sequence. To take full advantage of this powerful tool, the challenge resides in the design of such molecular probes to achieve high target specificity and therefore low noise in the images. As researchers continuously refine and re-engineer these molecules to improve their specificity, the use of dedicated small-animal PET machines allow the researcher to carefully evaluate both new tracers and new animal models of disease in an efficient and economic manner prior to human use [11,14,15,61–65]. The use of small-animal PET eliminates interanimal variability often found in drug discovery, since each animal can act as its own control. These scanners are designed to be used with both rodent and primate models of disease.

The PET imaging section of this article will focus on the oncological applications of small animal imaging PET machines, which perhaps provides the best opportunity for development. However, it is worth noting that the use of such cameras have been reported for a wide variety of applications. Among these studies are longitudinal investigations of glucose metabolism in rat heart [66,67] and brain [68–70], investigations into the dopaminergic system of the brain [71–74], as well as diseases of the brain such as epilepsy [75]. The most recent application of small-animal PET technology has appeared in the field of understanding non-oncological diseases. In the study of rheumatoid arthritis, Wipke and colleagues demonstrated the dynamic visualisation of a joint-specific autoimmune response, where ^{64}Cu-radiolabelled anti-glucose-6-phosphate isomerase IgG localised specifically in diseased distal joints within minutes of administration [76]. A flow tracer, ^{64}Cu-pyruvaldehyde-bis(N^4-methylthiosemicarbazone) (Cu-PTSM) has been used to label cells *ex vivo* for *in vivo* PET imaging of cell trafficking. Cu-PTSM was used to label $CD4^+$ T cells, to monitor the biochemical processes associated with inflammatory eye diseases such as Acute Autoimmune Uveitis with microPET [77]. The field of small-animal PET research is relatively new and commercial systems have only been available in the last few years. As such, the literature available on such studies is limited, but this by no means reflects the huge extent to which small-animal PET imaging is being used, the constant advances being made and the wealth of information being generated.

4.1. Instruments for small-animal PET

Since the recent commercial availability of complete small-animal tomographs, small-animal PET imaging is no longer restricted to research centres having the human resources and physical infrastructure to develop cameras. However, several institutions have continued to develop their own systems, and in doing so have demonstrated extreme originality from both the physicists and chemists. This section comprises a short survey of PET tomographs dedicated to small animal imaging and will briefly describe the cameras currently in use or in construction in different laboratories throughout the world. A similar survey has recently been published and the reader is referred to this publication for complementary information [61]. Since a complete description of every system would be too long, only the principal characteristics will be presented. Performance of the cameras will be described using published or reported values of spatial resolution and absolute sensitivity only. However, a complete assessment of the camera performance should not be limited to these measurements. The reader is referred to the cited publications, and references therein, for more details.

The University of California Los Angeles (UCLA) Crump Institute has a long history of PET detector and PET camera development. A complete account of the contribution of this laboratory to clinical PET and to small animal PET is beyond the scope of this article and, therefore, in this article we will focus on the UCLA small-animal PET [78,79]. The design adopted for this instrument is that of a full-ring camera consisting of 30 detector modules. Each module was designed around the concept of a small array of scintillation crystal coupled to a position sensitive photo-multiplier tube (PS-PMT) though a coherent bundle of optical fibres [80]. The scintillation material is made of Lutetium Oxyorthosilicate (CTI Knoxville, TN, USA) (LSO), an emerging fast scintillation crystal, characterised by a light scintillation constant of 40 ns and a light emission of 75% that of NaI [81], arranged in an 8×8 array of individually cut crystals each having the dimensions of $2\times2\times10$ mm. Due to the size of the phototube, a 24-cm long bundle of fibre optics is employed and these optical fibres create a one to one coupling between each element of the crystal array and each channel of the multichannel PS-PMT. Thirty of these modules are arranged in a ring conferring a ring diameter of 17.2 cm and an axial field of view (FOV) of 1.8 cm. The spatial resolution of the array is 1.8 mm isotropic in the centre of the FOV and is uniform with a value of 2 mm in the central 3 cm of the FOV. An absolute sensitivity of 200 counts per second (cps)/μCi or 0.56% was reported using a lower energy acceptance limit set to 250 keV.

A commercial version of this camera is currently produced by Concorde MicroSystems Inc. (Knoxville, TN, USA). This company specialises in the design of Application Specific Integrated Circuits (ASIC) and has been involved since 1992 in the development of components for clinical PET cameras. More recently. this company has been engaged in the construction and commercialisation of a complete small animal PET camera, with the UCLA microPET serving as the prototype for their design. The commercial versions, available in two models, rodent and primate, uses the concept of a small array of scintillation crystals coupled to a PS-PMT via a bundle of optical fibre. The Concorde models differ in several aspects from the prototype; a different choice of PS-PMT allowed the manufacturer to use a shorter fibre optic light guide, which in turn permitted a closer packing of the detectors. These cameras are built with four rings of 24 detectors for the rodent or 40 detectors for the primate model. This increased axial coverage resulted in a significant increase of absolute sensitivity, reaching 2.7 and 2.2% for the rodent and primate model, respectively [82]. The crystal size, slightly bigger than the original prototype, produced a spatial resolution slightly lower than the UCLA prototype. A value of 1.8 mm at the centre of the FOV was reported, but this value was seen to increase rapidly to slightly less than 2.5 mm, at a radial distance of 1 cm [82]. The camera is equipped with a rotating point source (Ge-68) used for normalisation and attenuation correction.

The Quad-HIDAC (Oxford Positron System) [83], also available commercially, uses the Multi-Wire Proportional Chamber technology (MWPC) in addition to a High Density Avalanche Chamber (HIDAC). The HIDAC technology is well proven and has been in use for autoradiography in many laboratories for several years. The Quad-HIDAC is composed of laminated plates of interleaved lead and insulating sheets mechanically drilled with a dense matrix of small holes (0.5 mm). The annihilation photons from the isotope emission will mainly result in ionisation from the interaction with electrons in the lead plates. The ejected electrons are then accelerated in the holes, and collected by an array of anode wires. Finally, they induce a signal in an array of cathode strips on the lead face. The intrinsic resolution is determined by the hole-pitch and the sensitivity is determined by the interaction probability with the lead. Four modules (a module consisting of a stack of parallel plates) are placed to enclose a FOV of dimensions 17×28 cm. Rotation of the four modules around the subject allows for the complete tomographic data acquisition. This camera offers sub-millimetre spatial resolution with an absolute sensitivity of 1.8% being reported.

The TierPET [84,85] and YAPPET [86,87] are similar cameras using Yttrium Aluminum Perovskite (YAP) scintillators which were separately developed at both the University of Julich, Germany (TierPET) and University of Ferrara, Italy (YAPPET). These cameras are built with four arrays of small finger-like scintillation

crystals coupled to a PS-PMT mounted on a rotating ring. The detector spacing can be adjusted to accommodate different animal sizes and the detector rotates around the animal-subject to acquire a complete tomographic data set. The crystal array of the TierPET is made of 2×2×15 mm YAP crystals in a 20×20 array. The YAPPET camera uses longer crystals (30 mm) in a similar configuration. The highlights of the reported performance of the TierPET can be summarised by a spatial resolution of 2.1 mm in the centre of the FOV and sensitivity of 0.32%. The YAPPET reported a similar spatial resolution, but a sensitivity of 1.7%. This higher value was obtained by setting the lower energy limit for gamma acceptance to 50 keV.

The National Institutes of Health (Bethesda, MD, USA) have developed a small animal PET camera, ATLAS, with a depth of interaction capability [88]. This camera is composed of 18 detector modules arranged in an 11.8 cm diameter ring. Each module is made of two 9×9 arrays placed back-to-back. The dual layer scintillator crystal arrays (each crystal having dimension of 2 mm×2 mm) are optically coupled to a PS-PMT. The total crystal depth is 15 mm and the front crystal is made of LGSO and the back is made of GSO. Since the decay times of the crystal materials are different (60 ns versus 40 ns), the single PMT signal is used to determine in which crystal the interaction occurred. A spatial resolution of 2 mm in the centre has been measured and an absolute sensitivity of 1.6% has being reported. This NIH system followed a previous version composed of two stationary opposed crystal arrays coupled to a positron-sensitive PMT [89]. In this instrument, the detectors were made of an array of 26×22 (2×2×10 mm) bismuth germanate (BGO) crystals directly coupled to a PS-PMT. The system was equipped with a rotator used to rotate the animal being imaged in order to get complete tomographic projections.

The VUB-PET [90–92] constructed at the University of Brussels in Belgium is an animal PET camera combining BaF_2 scintillator material with a photosensitive gas. In this camera, the annihilation photons interact with a BaF_2 scintillator array. The crystal size is 3×3×20 mm. Upon the photoelectric or Compton interaction with the crystal, the subsequent emission of ultra-violet light will ionise TMAS vapour in a conversion gap of a gas detector, with the electrons drifting towards a two-stage amplification chamber. Positron detection is performed by using an array of anodic wires. The overall camera contains 2060 BaF_2 crystals arranged in a cylinder measuring 20 cm diameter and 5.2 cm long. The transaxial FOV is limited to 11 cm. A spatial resolution of 2.6 mm in the centre has been reported and the absolute sensitivity at the centre of the FOV has been measured to be 30 kcps/MBq or 3%. This high sensitivity was acquired using a low energy threshold due to the poor energy resolution of this detector design.

Massachusetts General Hospital has built a single-plane PET tomograph having a spatial resolution approaching 1 mm [93]. The single-ring camera is composed of 360 LSO crystals with a light output readout of 30 PMT. The crystal dimensions are small (1×4.5×5 mm) in order to reduce the degradation of resolution due to multiple detector penetration from photons with incident angles far from normal angles and to reduce the blurring due to multiple interaction sites inside one crystal. This choice of crystal size resulted in a compromised sensitivity. The reported reconstruction spatial resolution is 1.25 mm in the centre of the FOV, and 1.75 mm at 2.5 cm away from the centre. An absolute sensitivity is reported to be only 30 cps/μCi or 0.008%, which is due to the small crystal size and the limited spatial resolution of the tomograph.

Indiana University has constructed an animal PET, the IndyPET, composed of two detector banks mounted on a rotating gantry [94]. The separation distance between these banks is adjustable between 22 and 42 cm. Each bank contains eight Siemens/CTI HR detector blocks. Each block is cut into a 7×8 array, with a light output readout from 4 PMT. The FOV is 18 cm transaxially and 5 cm axially with a spatial resolution of 2.8 mm in the centre of the FOV. This value increases to slightly less than 3.4 mm at 1 cm away from the centre of the FOV, for any detector separation value. The camera operates in step-and-shoot mode, during camera rotation, to acquire a complete tomographic dataset. This camera has recently been upgraded and now includes four detector banks for an increased sensitivity [95].

The PMT has dominated the field of nuclear medicine since its inception. Despite the progress made in PMT technology, the tube has essentially remained unchanged since its invention in 1947. The principal advantage of the tube is its high gain and speed. High gain, i.e. the ability to convert a weak luminous signal into a measurable electrical pulse is a necessary attribute. The disadvantages of the phototube are size, gain stability over time and temperature changes. The only current contender to replace the phototube is the Avalanche Photodiode (APD). This device is a photosensitive semiconductor showing excellent characteristics in high quantum conversion efficiency and small size. Amplification gain factors of the order of 1000 have been measured, but more typically gains of a few hundreds are observed. These gain factors are to be compared with a gain of the order of 10^6 in PMT tubes. However, such gains are high enough for the detection of scintillation light from 511 keV photons. Recent progress in APD technology has triggered a lot of activity in the design and development of small animal PET tomographs, and it is likely that the next version of commercial cameras will be based on this technology.

The Sherbrooke University (Sherbrooke, Canada) small animal PET camera was the first tomograph built

using the APD technology [96]. It is composed of two rings of 256 BGO crystals with individual APD light readouts. The crystal dimensions are 3×5×20 mm individually coupled to an APD. The overall ring diameter is 31 cm and the axial FOV is 1.05 cm. The system employs 'clam shell' motion of the detector rings to achieve greater linear spatial sampling. This camera is characterised by a reconstructed spatial resolution of 2.1 mm at the centre of the FOV. Due to the limited axial extent of the FOV, a low sensitivity has been observed 0.4%.

The Munich (MAD-PET) prototype [97,98] was initially composed of two detector heads, subsequently extended to six detector heads, using 2×8 arrays of LSO optically coupled to 2×8 multi-channel APD. This prototype led the same institution to develop a two-layer APD based full-ring tomograph [99]. This camera is made of very compact PET detector modules composed of two layers. Each module is made of two arrays of 4×8 LSO crystals (2×2×6 mm) with light output readouts utilising a novel monolithic array of densely packed APDs. The two arrays are placed back-to-back to increase sensitivity and to provide a depth of interaction capability.

Other cameras like the UCLA animal PET (ECAT-713) [100], Hamamatsu SHR-2000 [101] and SHR-7700 [102] and the Hammersmith RAT-PET [103,104] were also developed, mostly for primates imaging, and will not be described in detail here. Phillips Medical System may eventually release a small animal camera consisting of a small sized GSO crystal coupled to a continuous light guide with light readout with an array of PMT. The common performance characteristics in the previously described cameras is that they can be characterised by a spatial resolution of 2 mm or greater. These cameras, which can be described as being from the first generation of small animal PETs, are suitable for imaging mice, rats and small monkeys. The UCLA group is now working on the completion of the microPET-II [105]. This camera is based on the same design concept of the first generation of microPETs using an array of small sized scintillation crystals coupled to a PS-PMT through optical fibres. Presentation of characteristics and performance are expected later this year. Several other new PET detector designs are being developed using PS-PMT or APD technology. A few examples include the CLEAR PET project from the Crystal Clear Collaboration using the recently developed scintillation crystals made of LuAP (Lutetium Aluminum Perovskite) from CERN. The University of Seattle has developed PET detector modules made from an array of MLS (Mixed Lutetium Silicate, Vancouver, Canada)—Mice2—and from a continuous block of MLS coupled to a PS-PMT—cMiCE. Assembly into a complete imaging system is presently in progress.

4.2. Imaging of gene expression

Carefully designed radiolabelled molecular probes can target reporter gene expression and as such provide the opportunity to combine molecular biology and molecular imaging. The basic principle of imaging gene expression is simply that following the expression of a protein by a reporter gene, this protein will specifically bind to a positron-emitting radiolabelled probe (or PET reporter probes (PRG)) that has been administered to the animal. The gene of interest is always expressed along with the reporter gene, since the same promoter drives them both. Quantification of the amount of tracer retained by the expressed protein is directly proportional to the amount of protein expressed and therefore the level of gene expression. In basic research, this allows the investigator to non-invasively monitor the levels of genes expressed, the time course of expression, as well as the location of genes in transgenic models *in vivo*, as well as to monitor the efficacy of gene therapy protocols prior to human use. This exciting area has attracted increasing interest and has been recently and extensively reviewed [106–109].

The Crump Institute for Molecular Imaging is the world leader in the imaging of gene expression [110–113]. They have demonstrated that 8-[^{18}F]fluoroganciclovir (FGCV) is a substrate for the herpes simplex virus 1 thymidine kinase enzyme (HSV1-TK) and have imaged the gene expression in normal mice [113]. They have used the same tracer to image tumour cells transfected with a mutant herpes simplex virus (HSV1-sr39TK) as the PET reporter gene, which resulted in significantly enhanced sensitivity for imaging the gene expression [112]. In order to improve sensitivity, a direct comparison between a new probe, 8-[^{18}F]fluoropenciclovir (FPCV), and FGCV indicated that FPCV was a better probe than FGCV for imaging lower levels of HSV1-TK gene expression *in vivo* [111]. They further illustrated, in terms of potentially monitoring gene therapies, that microPET imaging of HSV1-sr39TK and dopamine-2-receptor reporter genes with 9-(4-[^{18}F]fluoro-3-hydroxymethylbutyl)guanine ([^{18}F]FHBG) and 3-(2-[^{18}F]fluoroethyl)spiperone ([^{18}F]FESP), utilising several adenovirus-mediated delivery routes, illustrated the feasibility of evaluating relative levels of therapeutic transgene expression in living animals [110].

4.3. Monitoring of therapy response

PET imaging has traditionally focused on the delineation of the uptake of a tracer in tissue as a direct measurement of a biological process. More recently, PET has become a tool as a surrogate marker for the action of therapeutic drugs. For example, an important aspect of receptor-based imaging agents is their use in the monitoring of conventional chemotherapy regimes

in cancer patients. In patients with primary and metastatic breast cancer, data obtained from PET imaging after 16-α-[^{18}F]fluoro-β-estradiol (FES) administration correlates with tumour oestrogen receptor status determined *in vitro* [114]. Comparison studies showed that fluorine-labelled deoxyglucose (FDG) was more sensitive than FES in staging breast cancer, and those patients who are oestrogen receptor-positive (ER+) by *in vitro* assays, but FES-negative may be less likely to respond to hormonal therapy [115]. Oyama and colleagues have now extrapolated this basic principle, to monitor the effects of androgen therapy on prostate tumours using microPET [116]. The study was undertaken to determine whether PET imaging could evaluate early changes in tumour metabolism following androgen ablation therapy and the results indicated that changes in serum testosterone levels influence glucose metabolism in the prostate gland within 24 h of treatment.

Historically, the assessment of tumour geometry and volume has been by the use of caliper measurements. Not only is this mode of measurement limited by the tumour's irregular shape, it does not yield any physiological information during radiotherapy experiments. As shown by Lewis and colleagues, microPET images in conjunction with MR imaging yielded information and data not normally available with the use of caliper measurements [33]. This study demonstrated the therapeutic potential of a radiotherapeutic drug in inhibiting cancer cell attachment to incision sites and growth of metastasis following laparoscopy surgery. The results indicated microPET and MRI could help determine overall treatment effectiveness and monitor therapeutic response and, as such, form a powerful combination of imaging modalities that will find broad application in the characterisation of disease states and the development of therapeutics.

4.4. Receptor/antigen-specific agents

The overexpression of cell surface or nuclear receptors is the premise for receptor-based radiopharmaceuticals. In designing radiolabelled receptor ligands, selectivity, low non-specific binding and incorporation of the radionuclide are three factors to consider. High affinity for the receptor of interest and low affinity for other receptor systems improves selective tumour uptake. For receptor-based radiopharmaceuticals, one of the most important considerations is that the radionuclide placement does not significantly decrease the receptor binding of the original ligand. Receptor ligands can be larger biomolecules such as peptides, or smaller organic molecules such as dopamine or folic acid. The design of such agents involves careful consideration of multiple factors. The use of microPET to 'screen' new biomolecules in disease models during the developmental stage significantly speeds up the discovery process. There have been numerous publications and reviews on receptor-based radiopharmaceuticals for both imaging and therapy (e.g. Refs. [117–121]). The use of small animal imaging PET technology is now beginning to become involved in the development of novels compounds, some examples of which are highlighted here.

Successful imaging by radiolabelled antitumour antibodies has been limited by slow uptake in tumour tissues and poor clearance from non-target tissues. Hybridoma technology is now at the point where genetically engineered fragments of antibodies, with rapid access and high retention in tumorous tissues combined with excellent clearance properties, have made the use of such biomolecules suitable for employment in PET imaging. Wu and colleagues developed an engineered single-chain variable fragment from the high-affinity anticarcinoembryonic antigen (CEA) monoclonal antibody T84.66 [122]. The ^{64}Cu-labelled minibody was used to successfully image with microPET a CEA-positive tumour, laying the foundation for an application of the same compound in human studies. Clearly the detection of radiolabelled engineered fragments by microPET has potential for broad application in many areas of genomics, phage display and proteomics.

Over the last 15 years, considerable progress has been made in the investigation of radiolabelled somatostatin (sst) analogues as both imaging and radiotherapeutic agents for somatostatin receptor-positive tumours. A number of recent studies have focused on improving the target tissue uptake of radiolabelled somatostatin analogues [123–125]. A study by Li and colleagues using microPET has now demonstrated that DOTA-DY1-TATE, a somatostatin analogue, can be labelled with both metal and halogen radionuclides, and its ^{64}Cu- and ^{125}I radiolabelled compounds showed somatostatin receptor-mediated uptake in normal and tumour tissues [126]. A ^{66}Ga labelled analogue, DOTA-DPhe^{1}-Tyr^{3}-octreotide has also been evaluated by microPET and it was concluded that this compound could also be used for PET diagnosis and quantitative imaging-based dosimetry of sst-positive tumours [127].

4.5. Other agents

Cu-PTSM has been used to label cells *ex vivo* for *in vivo* PET imaging of cell trafficking in mice in order to eventually track the selective recruitment of specific immune cells during the pathogenesis of cancerous disease states [128]. This study similar to that discussed earlier [77] has demonstrated the feasibility of monitoring *in vivo* cell migration with microPET systems.

A study from Washington University has investigated the potential of agents for bone imaging using microPET that will have application in the imaging of bone metastasis. The significant bone uptake of ^{64}Cu-1,4,7,10-tetraazacyclododecane - 1,4,7 - *tri*(methanephosphonic

acid) (DO3P) in microPET imaging studies was consistent with the biodistribution data for this agent. Comparative microPET studies demonstrated that ^{64}Cu-DO3P showed more optimal bone images than ^{94m}Tc-medronate and comparable images to $^{18}F^-$ in rats, which was further confirmed by the dynamic bone-imaging studies in mice [129].

4.6. Co-registration

For those studies involving highly specific molecular probes targeting a small population of cells, investigators have often found the PET images hard to interpret due to the lack of anatomical landmarks. For studies that involve kinetic modelling, the investigators also found the current attenuation correction mechanism incapable of providing the level of quantitative accuracy needed. Another need for high anatomical information comes from the necessity for an accurate phenotyping of animal models in order to stratify the animals in experimental groups prior to microPET imaging. Such examples could be for determining the presence of endometrial cancer in mice or for the determination of cardiac volume. The images obtained from the microPET scanner often become difficult to interpret due to the lack of anatomical landmarks. A good example is in the imaging of a therapeutic agent designed to target only the cancerous cells. Carefully following its biological distribution in an animal over an extended period of time, one can establish the pharmacokinetics of the new drug and accelerate the development cycle time. Unfortunately, we often see a highly localised uptake of such agents without knowing its exact anatomical location in the animal. Furthermore, it is difficult to assess the tumour volume from microPET images alone without sacrificing the animal. It is becoming apparent that high-resolution anatomical images are a necessity for the accurate interpretation of certain PET studies. Furthermore, properly registered anatomical images may improve the accuracy of microPET images with better attenuation correction. Therefore, there is a need to develop co-registration methods between microPET imaging with MRI and/or CT. Researchers will then be able to identify better tumour size and location, measure the standard uptake values in small organs or tumours, and to improve the quantitative assessment of tumour or animal models. Prior knowledge of small-size organs may also provide correction for partial volume effects, or even improve image resolution with statistical reconstruction methods.

5. Optical imaging

Advances in optical technologies have re-ignited interest in optical imaging as a powerful tool for biomedical application. Biomedical optical imaging uses propagating light to activate chromophores in tissues and a detector to capture the transmitted or reflected photons [130,131]. Planar optical images are frequently obtained by using a charge-coupled device (CCD) camera, and with advances in sophisticated image reconstruction algorithms, high-resolution 3D images in real time will soon become a reality [132,133]. Biomedical optical methods provide distinctly new diagnostic capabilities while complementing conventional imaging modalities [134–138]. Some advantages of optical imaging methods include the use of non-ionising low energy radiation, high sensitivity with the possibility of detecting micron-sized objects, capability of continuous data acquisition for real-time monitoring, and the development of potentially cost-effective equipment. It also provides flexibility in the mode of chromophore excitation (broadband light source, modulated light, continuous wave or pulsed laser) and signal detection (transillumination or reflectance, and scattering, absorption or fluorescence modes). Optical imaging methods can be completely non-invasive, especially when endogenous chromophores are used; minimally invasive, when contrast agents are injected; or invasive, when used in conjunction with surgical procedures or catheterisation.

Two fundamental properties of tissue optics that depend on the wavelength (light scattering and absorption in turbid media) affect both image resolution and depth of light penetration in tissues. In the ultraviolet and visible regions, scattering and absorption of light by photoactive intrinsic biomolecules limit its tissue penetration to a few millimetres. Thus, optical imaging in these regions is conventionally used to evaluate cutaneous lesions, endoscope-accessible and surgically exposed deep tissues. At the near infrared (NIR) region between 700 and 900 nm, absorption by intrinsic photoactive biomolecules is low and allows light to penetrate several centimetres into tissue, a depth that is sufficient to image practically all small animals without resorting to expensive and sophisticated imaging techniques. A typical apparatus for optical imaging of small animals is shown in Fig. 1 [139,140]. Generally, the animal fur in the region of interest is shaved to minimise light reflections. The abundance of endogenous and exogenous photoactive molecules enables the imaging of animals with the aid of several optical contrast effectors. While several clinical studies with human subjects have been reported, the remaining part of this section will focus on optical imaging of animals for oncology purposes.

5.1. Animal imaging with endogenous (intrinsic) optical contrast effectors

Several naturally occurring and intrinsic molecules are photoactive in the UV, visible and infrared wavelengths

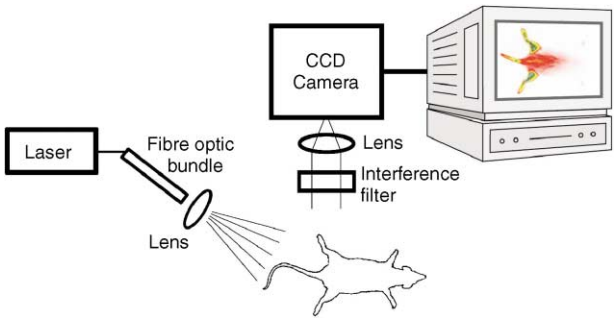

Fig. 1. Fluorescence imaging system for detecting superficial tumours. CCD, charge-coupled device.

and this feature generates optical contrast useful for the diagnosis of various pathological conditions. The major endogenous chromophores are aromatic amino acids, DNA, proteins, melanin, and enzyme co-factors in the UV region; haemoglobin, myoglobin, bilirubin, and some enzyme cofactors in the visible region; and water and fat in the NIR region. Broadband chromophores such as melanin and haemoglobin have extended absorption into the visible and NIR regions, respectively. Small animal imaging with the aid of endogenous contrast effectors is typically performed by reflectance spectroscopy, employing any of the fluorescence, absorption or Raman scattering detection techniques [141]. The shallow penetration of light in the UV and visible wavelengths limits the application of this approach to the evaluation of superficial tissues such as skin diseases [142–145] and the gastrointestinal systems by endoscopy [141]. Some studies have used NIR optical tomography to image deep tissues with the aid of endogenous contrast effectors. This approach relies on the differential ratio of oxyhaemoglobin and deoxyhaemoglobin in normal and pathological tissues to localise abnormal conditions such as tumours. The use of a non-invasive protocol and medically safe laser power has facilitated the application of NIR optical tomography in human subjects for imaging brain function [146] and breast tumours [147–150]. Imaging of small animals by intrinsic chromophore-mediated contrast represents a viable, non-invasive approach to monitor various disease states, quantify pathologically relevant physiological functions, and localise cancer. However, deciphering the spectral properties of normal and pathological tissues based on endogenous contrast, especially at the onset of abnormality, remains difficult, despite the availability of sophisticated image reconstruction algorithms.

5.2. Animal imaging with exogenous (extrinsic) optical contrast agents

As with other imaging modalities, optical imaging benefits from the use of exogenous contrast agents to increase the sensitivity and specificity of its diagnostic potential. Contrast agents are less dependent on inter- and intraspecies variations, and can furnish unique information regarding the functional status of tissues. In addition to enhancing tissue contrast, such agents also promote rapid selective localisation, improve specificity and sensitivity, and may provide important histopathological information such as cell viability. Any biocompatible molecule that absorbs, emits, or scatters light of an appropriate wavelength can serve as an optical contrast agent. Currently, most optical probes used for animal imaging rely on absorption or fluorescent characteristics of the agent, although recent advances in the production of biocompatible particulates promises to provide reliable scattering optical contrast. In general, fluorescein, indocyanine green (ICG) and porphyrin derivatives are widely used as optical contrast agents for *in vivo* imaging. Representative optical contrast agents for imaging tumours in animals are listed in Table 1. These agents localise in pathological tissues by different mechanisms as discussed below.

5.2.1. Non-specific imaging agents

Indocyanine green (ICG) is the major non-specific optical contrast agent used for animal and human imagng studies, probably because of its established safety profile in humans [131,137,139,151]. ICG absorbs and fluoresces in the NIR region, a feature that is essential for whole-body small-animal imaging. Detection of cancer by non-specific agents such as ICG relies on the differential accumulation of the agent in the pathological tissue based on impaired tumour capillary permeability, increased interstitial fluid, or other structural changes. ICG has successfully been used to diagnose cancers in humans [137,152,153] and animals. For example, Reynolds and colleagues demonstrated the potential to image spontaneous canine mammary tumours with ICG by frequency domain photon migration fluorescence imaging [151]. Although ICG is a good model for many small-animal and human cancer studies, it is rapidly cleared by the liver's first pass effect. This requires that non-specific localisation of ICG in the tumour be rapid, unless a continuous infusion method is utilised. However, the development of a novel non-tumour-specific ICG derivative with improved pharmacokinetics may overcome the problem with rapid ICG elimination from the circulation during small-animal imaging [154]. While the non-specific nature of ICG permits its use to screen a variety of tumours, the probe is equally retained in a host of non-tumour related injuries that result in false-positive data. Similarly, non-specific agents are not reliable for detecting tumours. A recent comparison of the retention of ICG in rats bearing cancer cells of different origins showed sporadic uptake in some tumours and not in others, a situation that results in increased false-negative

Table 1
Representative optical contrast agents for animal imaging

Species	Tumour	Contrast effector	Retention mechanism	Ref.
Rat	Neuroendocrine	Cyanine-octreotate	Sst_2 receptor-specific	[139]
Mouse	Neuroendocrine	Cyanine-octreotate	Sst_2 receptor-specific	[163]
Rat	Neuroendocrine, Prostate	Cyanine-bombesin	Bbn receptor-specific	[140]
Mouse	Mammary, fibrosarcoma	Cyanine-graft co-polymer	Protease activity	[182,183,186]
Mouse	Metastatic, tumour angiogenesis, others	Green fluorescent protein	Gene expression	[184,185,187]
Mouse	Cervical	Luciferin	Luciferase activity	[188]
Rat	Glioma	Cyanine-sugar	Non-specific	[154]
Mouse	Colon	Cyanine-transferrin	Transferrin receptor	[189]
Dog	Mammary	ICG	Non-specific	[151]
Dog	Mammary	HPPH[a]-carotene	LDL-receptor	[181]
Dog	Mammary	HPPH-carotene	LDL-receptor	[181]
Rat	Prostate	ICG	Non-specific	[139]
Mouse	Larynx	Cyanine-MAb E48	MAb E48 receptor	[160]
Mouse	Colon	Fluorescein-CEA Mab	CEA receptor	[156]

[a] Sst_2, somatostatin (subtype-2); Bbn, bombesin; ICG, indocyanine green; HPPH, hexylpyropheophorbide; LDL, low-density lipoproteins; CEA, anti-human carcinoembryonic antigen monoclonal antibody; MAb, monoclonal antibody.

data [139]. Because of the low specificity and selectivity of non-specific probes, many studies are currently evaluating new site-specific agents for optical imaging by various delivery mechanisms [131,155].

5.2.2. Receptor-specific imaging agents

Facilitated by advances in molecular biology, numerous tumour cells are known to overexpress certain receptors that have become the target to deliver diagnostic or therapeutic agents [118]. Pioneering studies by this mechanism were mostly performed with radiolabelled antibody conjugates, that have been adopted for optical imaging of small animals [156–158]. Earlier studies focused on the use of fluorescein-antibody conjugates for optical imaging of tumours because of its ready availability, mild reaction condition, and the ease of observing tumour localisation, even with the naked eyes [156,159]. Due to the shallow penetration of blue light used for fluorescein-mediated studies, the tumour xenographs had to be positioned on a readily accessible tissue surface such as rabbit ear [159]. For NIR optical imaging, carbocyanine dye bioconjugates are widely used. Several animal studies show that labelling large biomolecules such as antibodies with carbocyanine derivatives enhances the delivery of the agent to target tissues by receptor-mediated mechanisms [157,158,160–162]. However, efficient targeting of tumour receptors with antibodies is hampered by many factors, including a low diffusion rate to tumours, rapid uptake by the liver, and the potential to elicit adverse immunogenic reactions.

An alternative method for the efficient delivery of optical probes to tumors was recently demonstrated with carbocyanine–somatostatin receptor–avid peptide conjugate [139]. Other studies have confirmed the validity of this approach [140,163]. Some advantages of the peptide-based approach include enhanced localisation in tumours and rapid clearance from non-target tissues. Typically, rat pancreatic acinar carcinoma (CA20948) expressing the sst_2 receptor was induced by the solid implant technique in the left flank area. This tumour line is widely used for sst_2 receptor-positive assays, and the number of binding sites for somatostatin has been estimated as 489 fmol mg^{-1} [164]. Achilefu and colleagues [139,140] demonstrated that the optical contrast agents are selectively retained in tumour that overexpress the target receptor, indicating that the peptide retained its receptor binding affinity without loss of the optical probe's photophysical properties. A representative optical image obtained with a simple continuous wave fluorescence imaging system is shown in Fig. 2 [139,140].

Photodynamic therapy (PDT) agents represent another class of photoactive molecules that are preferentially retained in various types of tumours. Several reports suggest that the mechanism of tumour uptake is mediated by low-density lipoprotein (LDL) receptors, which are overexpressed in tumours [165–172]. Coupled with active LDL receptor uptake, the fluorescence properties of some PDT agents are utilised for the optical imaging of tumours in animals [138,173–181]. The PDT agents are usually formulated directly or conjugated with LDL-avid molecules before *in vivo* administration.

5.2.3. Functional imaging agents

The next frontier in optical imaging resides in the ability to probe biochemical activities *in vivo* and correlate the data with pathological conditions. In a pioneering study by Weissleder and colleagues [182], the

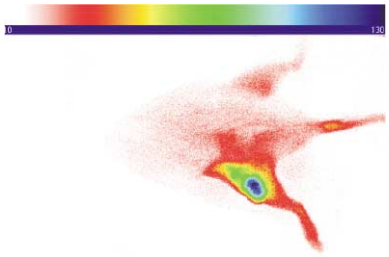

Fig. 2. Fluorescent image of NIR cyanine–somatostatin–avid peptide conjugate in a CA20948 tumour-bearing rat at 27 h postinjection. NIR, near infrared.

fluorescence of a prequenched optical probe was re-established on cleavage of protease-specific amino acid sequences incorporated into the probe. Recent studies demonstrate the potential use of this approach to diagnose and monitor the status of tumours by optical methods [183]. While this method offers enormous benefit for the early detection of cancer by monitoring aberrant gene expression, the large size of the co-polymer-probe conjugate used may preclude rapid delivery of the probe to tumours. It is also hoped that, for translational research purposes, the level of protease expression in aberrant cells in human subjects is within the detection limit of current optical imaging devices.

5.3. Others

Other important approaches for small animal optical imaging rely on bioluminescence or high-resolution optical coherence tomography methods. These approaches are described by Contag and Fujimoto in this Special Issue of the *European Journal of Cancer* and will not be considered here. Green fluorescent protein (GFP) is also a useful optical probe to image and monitor the status of various forms of cancer and metastasis in animals [184,185]. The procedure generally involves transduction of the *GFP* gene into human tumour lines and subsequent subcutaneous injection or orthotopic implant of the stable transductants into nude mice. Exciting the protein with a blue light and detecting the ensuing fluorescence with a CCD camera enables the whole body imaging of GFP expression in animals. The absorption and fluorescence of GFP in the visible region, coupled with the increased light scattering, may hinder the use of GFP for high-resolution imaging of deep tissues.

6. Summary

Advances in the biomedical sciences have been accelerated by the introduction of many new imaging technologies in recent years including PET and optical imaging. With animal models widely used in the basic and preclinical sciences, finding ways to conduct animal experiments more accurately and efficiently becomes a key factor in the success and timeliness of oncological research. Non-invasive imaging technologies will prove to be valuable tools in conducting timely oncological research.

Acknowledgements

Small Animal Imaging at Washington University is supported by an NIH/NCI SAIRP grant (1 R24 CA83060). We would also like to thank the Small Animal Imaging Core of the Alvin J. Siteman Cancer Center at Washington University and Barnes-Jewish Hospital in St. Louis, MO for additional support of the small animal imaging. The Core is supported by an NCI Cancer Center Support Grant # 1 P30 CA91842.

References

1. Budinger TF, Beneron DA, Koretsky AP. Imaging transgenic animals. *Annu Rev Biomed Eng* 1999, **1**, 611–648.
2. Weissleder R. Scaling down imaging: molecular mapping of cancer in mice. *Nature Rev* 2002, **2**, 1–8.
3. Borah B, Gross GJ, Dufresne TE, *et al*. Three-dimensional microimaging (MRmicroI and microCT), finite element modeling and rapid prototyping provide unique insights into bone architecture in osteoporosis. *Anat Rec* 2001, **265**, 101–110.
4. Rietbergen van B, Majumdar S, Pistoia W, *et al*. Assessment of cancellous bone mechanical properties from micro-FE models based on micro-CT, pQCT and MR images. *Technol Health Care* 1998, **6**, 413–420.
5. Ruegsegger P, Koller B, Muller R. A microtomographic system for the non-destructive evaluation of bone architecture. *Calcif Tissue Int* 1996, **58**, 24–29.
6. Kennel SJ, Davis IA, Branning J, Pan H, Kabalka GW, Paulus MJ. High resolution computed tomography and MRI for monitoring lung tumor growth in mice undergoing radioimmuntherapy: correlation with histology. *Med Phys* 2000, **27**, 1101–1107.
7. Paulus MJ, Gleason SS, Sari-Sarrat H, *et al*. High-resolution X-ray CT screening of mutant mouse models. *Proc SPIE* 2000, **3921**, 270–279.
8. Paulus MJ, Gleason SS, Kennel SJ, Hunsicker PR, Johnson DK. High resolution X-ray computed tomography: an emerging tool for small animal cancer research. *Neoplasia* 2000, **21**, 62–70.
9. Paulus MJ, Gleason SS, Easterly ME, Foltz CJ. A review of high-resolution X-ray computed tomography and other imaging modalities for small animal research. *Lab Animal* 2001, **30**, 36–45.
10. Weber DA, Ivanovic M, Franceschi D, *et al*. Pinhole SPECT: a new approach to in vivo high resolution SPECT imaging in small animal laboratory animals. *J Nucl Med* 1994, **35**, 342–348.
11. Weber DA, Ivanovic M. Ultra-high-resolution imaging of small animals: implications for preclinical and research studies. *J Nucl Cardiol* 1999, **6**, 332–344.
12. Weisenberger AG, Bradley E, Majewski S, Saha M. Development of a novel radiation imaging detector system for *in vivo* gene imaging in small animal studies. *Conf Rec 1996 Med Imag Conf* , 1996, 1201–1205.
13. Wirrwar A, Schramm N, Vosberg H, Muller-Gartner HW. High resolution SPECT in small animal research. *Rev Neurosci* 2001, **12**, 187–193.

14. Green MV, Seidel J, Vaquero JJ, Jagoda E, Lee I, Eckelman WC. High resolution PET, SPECT and projection imaging in small animals. *Comput Med Imag Graph* 2001, **25**, 79–86.
15. Ploux L, Mastrippolito R. In vivo radiolabel quantification in small-animal models. *Nucl Med Biol* 1998, **28**, 737–742.
16. Rooks V, Beecken W-D, Iordanescu I, Taylor GA. Sonographic evaluation of orthotopic bladder tumors in mice treated with TNP-470 an angiogenic inhibitor. *Acad Radiol* 2001, **8**, 121–127.
17. Zagar B, Fornaris R, Ferrera K. Ultrasonic mapping of the microvasculature: siganl alignment. *Ultrasound Med* 1998, **24**, 809–824.
18. Kish PE, Blaivas M, Strawderman M, Muraszko KM, Ross DA, Ross BD. G. M. Magnetic resonance imaging of ethylnitrosourea-induced rat gliomas: a model for experimental therapeutics of low-grade gliomas. *J Neuro-Oncol* 2001, **53**, 243–257.
19. Schabet M, Martos J, Buchholz R, Pietsch T. Animal model of human medulloblastoma: clinical, magnetic resonance imaging, and histopathological findings after intra-cisternal injection of MHH-MED-1 cells into nude rats. *Med Pediatric Oncol* 1997, **29**, 92–97.
20. Martinez DA, Kahwash S, O'Dorisio MS, Lloyd TV, McGhee RBJ. Disseminated neuroblastoma in the nude rat. A xenograft model of human malignancy. *Cancer* 1996, **77**, 409–419.
21. Vertrees RA, Deyo DJ, Quast M, Lightfoot KM, Boor PJ, Zwischenberger JB. Development of a human to murine orthotopic xenotransplanted lung cancer model. *J Invest Surg* 2000, **13**, 349–358.
22. Pulkkanen KJ, Parkkinen JJ, Kettunen MI, *et al*. Characterization of a new animal model for human renal cell carcinoma. *In Vivo* 2000, **14**, 393–400.
23. Xiao Z, McCallum TJ, Brown KM, *et al*. Characterization of a novel transplantable orthotopic rat bladder transitional cell tumour model. *Br J Cancer* 1999, **81**, 638–646.
24. Abdulkadir SA, Qu Z, Garabedian E, *et al*. Impaired prostate tumorigenesis in Egr1-deficient mice. *Nat Med* 2001, **7**, 101–107.
25. He Z, Evelhoch JL, Mohammad RM, *et al*. Magnetic resonance imaging to measure therapeutic response using an orthotopic model of human pancreatic cancer. *Pancreas* 2000, **21**, 69–76.
26. Saini M, Bellinzona M, Weichhold W, Samii A. A new xenograft model of primary central nervous system lymphoma. *J Neuro-Oncol* 1999, **43**, 153–160.
27. Chenevert TL, Stegman LD, Taylor JM, *et al*. Diffusion magnetic resonance imaging: an early surrogate marker of therapeutic efficacy in brain tumors. *J Natl Cancer Inst* 2000, **92**, 2029–2036.
28. Poptani H, Puumalainen A-M, Grohn OH, *et al*. Monitoring thymidine kinase and ganciclovir-induced changes in rat malignant glioma in vivo by nuclear magnetic resonance imaging. *Cancer Gene Ther* 1998, **5**, 101–109.
29. Jennings D, Hatton BN, Guo J, *et al*. Early response of prostate carcinoma xenografts to docetaxel chemotherapy monitored with diffusion MRI. *Neoplasia* 2002, **4**, 255–262.
30. Beauregard DA, Pedley R, Barbara H, Sally A, Brindle KM. Differential sensitivity of two adenocarcinoma xenografts to the anti-vascular drugs combretastatin A4 phosphate and 5,6-dimethylxanthenone-4-acetic acid, assessed using MRI and MRS. *NMR Biomed* 2002, **15**, 99–105.
31. Khandaker MH, Kadhim SA, Ischim TE, Howson-Jan K, Chin J, Sighal SK. Prevention of bladder tumor formation in mice by a novel bone marrow-derived factor, reptimed. *Anticancer Res* 2000, **20**, 183–189.
32. Cordel S, Dupas B, Douillard JY, Meflah K. Interleukin-2/sodium butyrate treatment cures rats bearing liver tumors after acquired 5-fluorouracil resistance. *Int J Cancer* 1998, **78**, 735–739.
33. Lewis JS, Connett JM, Garbow JR, Buettner TL, Fujibayashi Y, Fleshman JW, Welch MJ. Cu-64-pyruvaldehyde-bis(N^4-methylthiosemicarbazone) for prevention of tumor growth at wound sites following laparoscopic surgery: monitoring therapy response with microPET and magnetic resonance imaging. *Cancer Res* 2002, **62**, 445–449.
34. Su MY, Taylor JA, Villarreal LP, Nalcioglu O. Prediction of gene therapy-induced tumor size changes by the vascularity changes measured using dynamic contrast-enhanced MRI. *Mag Reson Imag* 2000, **28**, 311–317.
35. Stegman LD, Rehemtulla A, Hamstra DA, *et al*. Diffusion MRI detects early events in the response of a glioma model to the yeast cytosine deaminase gene therapy strategy. *Gene Ther* 2000, **7**, 1005–1010.
36. Fleige G, Nolte C, Synowitz M, Seeberger F, Kettenmann H, Zimmer C. Magnetic labeling of activated microglia in experimental gliomas. *Neoplasia* 2001, **3**, 489–499.
37. Fonchy E, Lahrech H, Francois-Joubert A, *et al*. A new gadolinium-based contrast agent for magnetic resonance imaging of brain tumors: kinetic study on a C6 rat glioma model. *J Mag Reson Imag* 2000, **14**, 97–105.
38. Prabhu SS, Broaddus WC, Oveissi C, Berr SS, Gillies GT. Determination of intracranial tumor volumes in a rodent brain using magnetic resonance imaging, Evans blue, and histology: a comparative study. *IEEE Trans Biomed Engin* 2000, **47**, 259–265.
39. Helbich TH, Roberts TP, Gossmann A, *et al*. Quantitative gadopentetate-enhanced MRI of breast tumors: testing of different analytic methods. *Mag Reson Med* 2000, **44**, 915–924.
40. Marinelli ER, Neubeck R, Song B, *et al*. Synthesis, characterization, and imaging performance of a new class of macrocyclic hepatobiliary MR contrast agents. *Invest Radiol* 2000, **35**, 8–24.
41. Konda SD, Aref M, Wang S, Brechbiel M, Wiener EC. Specific targeting of folate-dendrimer MRI contrast agents to the high affinity folate receptor expressed in ovarian tumor xenografts. *Magma* 2001, **12**, 104–113.
42. Wunderbaldinger P, Josephson L, Bremer C, Moore A, Weissleder R. Detection of lymph node metastases by contrast-enhanced MRI in an experimental model. *Mag Reson Med* 2002, **47**, 292–297.
43. Shahbazi-Gahrouei D, Williams M, Rizvi S, Allen BJ. In vivo studies of Gd-DTPA-monoclonal antibody and gd-porphyrins: potential magnetic resonance imaging contrast agents for melanoma. *J Mag Reson Imag* 2001, **14**, 169–174.
44. Maurer J, Strauss A, Ebert W, Bauer H, Felix R. Contrast-enhanced high resolution magnetic resonance imaging of pigmented malignant melanoma using Mn-TPPS4 and Gd-DTPA: experimental results. *Melanoma Res* 2000, **10**, 40–46.
45. Kiessling F, Fink C, Hansen M, *et al*. Magnetic resonance imaging of nude mice with heterotransplanted high-grade squamous cell carcinomas: use of a low-loaded, covalently bound Gd-Hsa conjugate as contrast agent with high tumor affinity. *Invest Radiol* 2002, **37**, 193–198.
46. Pilatus, U., Aboagye, E., Artemov, D., Mori, N., Ackerstaff, E., Bhujwalla, Z.M., Real-time measurements of cellular oxygen consumption, pH, and energy metabolism using nuclear magnetic resonance spectroscopy, Mag. Reson. Med., 45, 749–755.
47. Fan X, River JN, Zamora M, *et al*. Differentiation of nonmetastatic and metastatic rodent prostate tumors with high spectral and spatial resolution MRI. *Mag Reson Med* 2001, **45**, 1046–1055.
48. Bhujwalla ZM, Artemov D, Natarajan K, Ackerstaff E, Solaiyappan M. Vascular differences detected by MRI for metastatic versus nonmetastatic breast and prostate cancer xenografts. *Neoplasia (New York)* 2001, **3**, 143–153.
49. Leach MO. Application of magnetic resonance imaging to angiogenesis in breast cancer. *Breast Cancer Res* 2001, **3**, 22–27.
50. Tempel-Brami C, Neeman M. Non-invasive analysis of rat ovarian angiogenesis by MRI. *Mol Cell Endocrin* 2002, **187**, 19–22.

51. Verhoye M, van der Sanden BPJ, Rijken PFJW, *et al*. Assessment of the neovascular permeability in glioma xenografts by dynamic T(1) MRI with Gadomer-17. *Mag Reson Med* 2002, **47**, 305–313.
52. Maxwell RJ, Wilson J, Prise VE, *et al*. Evaluation of the antivascular effects of combretastatin in rodent tumours by dynamic contrast enhanced MRI. *NMR Biomed* 2002, 89–98.
53. Wang Z, Su MY, Najafi A, Nalcioglu O. Effect of vasodilator hydralazine on tumor microvascular random flow and blood volume as measured by intravoxel incoherent motion (IVIM) weighted MRI in conjunction with Gd-DTPA-albumin enhanced MRI. *Mag Reson Imag* 2001, **19**, 1063–1072.
54. Bjornerud A, Johansson LO, Ahlstrom HK. Pre-clinical results with Clariscan (NC100150 Injection); experience from different disease models. *Mag Reson Mater Phys Biol Med* 2001, **12**, 99–103.
55. Sato N, Kobayashi H, Hiraga A, *et al*. Pharmacokinetics and enhancement patterns of macromolecular MR contrast agents with various sizes of polyamidoamine dendrimer cores. *Mag Reson Med* 2001, **46**, 1169–1173.
56. Brasch R, Pham C, Shames D, *et al*. Assessing tumor angiogenesis using macromolecular MR imaging contrast media. *J Mag Reson Imag* 1997, **7**, 68–74.
57. Amorino GP, Lee H, Holburn GE, *et al*. Enhancement of tumor oxygenation and radiation response by the allosteric effector of hemoglobin, RSR13. *Radiat Res* 2001, **156**, 294–300.
58. Neeman M, Dafni H, Bukhari O, Braun RD, Dewhirst MW. In vivo BOLD contrast MRI mapping of subcutaneous vascular function and maturation: validation by intravital microscopy. *Mag Res Med* 2001, **45**, 887–898.
59. Al-Hallaq HA, Zamora M, Fish BL, Farrell A, Moulder JE, Karczmar GS. MRI measurements correctly predict the relative effects of tumor oxygenating agents on hypoxic fraction in rodent BA1112 tumors. *Int J Radiat Oncol Biol Phys* 2000, **47**, 481–488.
60. Robinson SP, Howe FA, Stubbs M, Griffiths JR. Effects of nicotinamide and carbogen on tumour oxygenation, blood flow, energetics and blood glucose levels. *Br J Cancer* 2000, **82**, 2007–2014.
61. Chatziloannou AF. Molecular imaging of small animals with dedicated PET tomographs. *Eur J Nucl Med* 2002, **29**, 98–114.
62. Cherry SR, Gambhir SS. Use of positron emission tomography in animal research. *J Clin Pharmacol* 2001, **41**, 482–491.
63. Hume SP, Jones T. Positron emission tomography (PET) methodology for small animals and its application in radiopharmaceutical preclinical investigation. *Nucl Med Biol* 1998, **25**, 729–732.
64. Myers R. The biological application of small animal PET imaging. *Nucl Med Biol* 2001, **28**, 585–593.
65. Myers R, Hume S, Bloomfield P, Jones T. Radio-imaging in small animals. *J Psychopharm* 1999, **13**, 352–357.
66. Lapointe D, Bentourkia M, Cadorette J, *et al*. High-resolution cardiac PET in rats. *J Nucl Med* 1999, **40**, 185P.
67. Kudo T, Annala AJ, Cherry SR, Phelps ME, Schelbert HR. Measurement of myocardial blood flow during occlusion/reperfusion in rats with dynamic microPET imaging. *J Nucl Med* 1999, **40**, 6P.
68. Kornblum HI, Araujo DM, Annala AJ, Tatsukawa KJ, Phelps ME, Cherry SR. In vivo imaging of neuronal activation and plasticity in the rat brain by high resolution positron emission tomography (microPET). *Nat Biotech* 2000, **18**, 655–660.
69. Moore TH, Osteen TL, Chatziioannou TF, Hovda DA, Cherry TR. Quantitative assessment of longitudinal metabolic changes in vivo after traumatic brain injury in the adult rat using FDG-microPET. *J Cereb Blood Flow Metab* 2000, **20**, 1492–1501.
70. Barrio JR, Toyokuni T, Gambhir SS, *et al*. In vivo imaging of neuronal activation and plasticity in the rat brain by high resolution positron emission tomography (microPET). *Nucl Med Biol* 2000, **27**, 157–162.
71. Qi J, Moore A, Annala A, *et al*. Deficits in striatal dopamine D(2) receptors and energy metabolism detected by in vivo microPET imaging in a rat model of Huntington's disease. *IEEE Trans Med Imag* 2000, **19**, 507–512.
72. Luthra SK, Brown DJ, Opacka-Juffry J, *et al*. The potential of high-resolution positron emission tomography to monitor striatal dopaminergic function in rat models of disease. *Nucl Med Biol* 1996, **23**, 377–384.
73. Torres EM, Hume SP, Myers R, *et al*. In vivo saturation kinetics of two dopamine transporter probes measured using a small animal positron emission tomography scanner. *Neuroscience* 1997, **79**, 711–721.
74. Sargent PA, Bench CJ, Rabiner EA, *et al*. Positron emission tomography (PET) methodology for small animals and its application in radiopharmaceutical preclinical investigation. *Neuroimage* 1998, **8**, 426–440.
75. Kornblum HI, Cherry SR. The use of microPET for the development of neural repair therapeutics: studies in epilepsy and lesion models. *J Clin Pharmacol* (Suppl) 2001, **41**, 55S–63S.
76. Wipke BT, Wang Z, Kim J, McCarthy TJ, Allen PM. Dynamic visualization of a joint-specific autoimmune response through positron emission tomography. *Nat Immunol* 2002, **3**, 336–372.
77. Wang Z, Sharp TL, Bora NS, *et al*. Approaches toward the in vivo imaging of experimental accute autoimmune uvitis (EAAU). *J Label Compd Radiopharm* 2001, **44**, S372–S373.
78. Chatziioannou AF, Cherry SR, Shao Y, *et al*. Performance evaluation of microPET: a high-resolution lutetium oxyorthosilicate PET scanner for animal imaging. *J Nucl Med* 1999, **40**, 1164–1175.
79. Cherry SR, Shao Y, Silverman RE, *et al*. MicroPET: a high resolution PET scanner for imaging small animals. *IEEE Trans Nucl Sci* 1997, **44**, 1161–1166.
80. Cherry SR, Yiping S, Siegel S, *et al*. Optical fiber readout of scintillator arrays using a multi-channel PMT: a high resolution PET detector for animal imaging. *IEEE Trans Nucl Sci, 1996, 43*.
81. Saoudi A, Pepin CM, Lecomte R. Study of light collection in multi-crystal detectors. *IEEE Trans Nucl Sci* 2000, **47**, 1634–1639.
82. Tai YC, Chatziioannou A, Siegel S, *et al*. Performacance evaluation of the microPET-P4: a PET system dedicated to animal imaging. *Phys Med Biol* 2001, **46**, 1845–1862.
83. Jeavons AP, Chandler RA, Dettmar CAR. A 3D HIDAC-PET camera with sub-millimeter resolution for imaging small animals. *IEEE Trans Nucl Sci* 1999, **46**, 468–473.
84. Weber S, Bauer A, Herzog H, *et al*. Recent results of the Tier-PET scanner. *IEEE Trans Nucl Sci* 2000, **47**, 1665–1669.
85. Weber S, Herzog H, Cremer M, *et al*. Evaluation of the TierPET system. *IEEE Trans Nucl Sci* 1999, **46**, 1177–1183.
86. Del Guerra A, Di Domenico G, Scandola M, Zavattini G. YAP-PET: first results of a small animal Positron Emission Tomograph based on YAP:Ce finger crystal. *IEEE Trans Nucl Sci* 1998, **45**, 3105–3108.
87. Del Guerra A, Damiani C, Di Domenico G, *et al*. First in vivo studies on rats with YAPPET scanner. In *Conference Proceedings IEEE NSS-MIC*. Seattle, WA, USA, 1999.
88. Siedel, J, Vaquero JJ, Green MV. Resolution uniformity and sensitivity of the NIH ATLAS small animal PET scanner: comparison to simulated LSO scanners without depth-of-interaction capability. In *Conference Proceedings IEEE NSS-MIC*. San Diego, CA, IEEE, 2001.
89. Siegel S, Vaquero JJ, Aloj L, *et al*. Initial results from a PET/planar small animal imaging system. *IEEE Trans Nucl Sci* 1999, **46**, 571–575.
90. Bruyndonckx P, Carnochan P, Yonggang W, *et al*. The VUB-PET system: performance evaluation and applications for radiotracer validation and anticancer drug development. In *Conference Proceedings; High Resolution Imaging in Small Animals*. Amsterdam, Netherlands, 1999.

91. Tavernier S, Bruyndonckx P, Shuping Z. A fully 3D small PET scanner. *Phys Med Biol* 1992, **37**, 635–643.
92. Tavernier, S, Brurndonckx P, Debruyne J, *et al*. First results from a prototype PET scanner isung BaF_2 scintillator and photosensitive wire chambers. In IEEE, ed. *Conference Proceedings IEEE NSS-MIC*, 1994.
93. Correia JA, Burnham CA, Kaufman D, Fishman AJ. Development of a small animal PET imaging device with resolution approaching 1mm. *IEEE Trans Nucl Sci* 1999, **46**, 631–635.
94. Rouze NC, Winkle W, Hutchins GD. IndyPET—a high resolution, high sensitivity dedicated research scanner. In *IEEE NSS-MIC*. Seattle, WA, 1999.
95. Rouze, NC, Stantz KM, Hutchins GD. Design of IndyPET-II, a high resolution, high-sensitivity dedicated research scanner. In *IEEE Nucl Sci Symp Med Imaging*. San Diego, CA, 2001.
96. Lecomte R, Cadorette J, Richard P, Rodrigue S, Rouleau D. Design and engineering aspects of a high resolution positron tomograph for small animal imaging. *IEEE Trans Nucl Sci* 1994, **41**, 1446–1452.
97. Pichler B, Boning G, Lorenz E, *et al*. Studies with a prototype high resolution PET scanner based on LSO-APD modules. *IEEE Trans Nucl Sci* 1998, **45**, 1298–1302.
98. Ziegler SI, Pichler BJ, Boening G, *et al*. A prototype high-resolution animal positron tomograph with avalanche photodiode arrays and LSO crystals. *Eur J Nucl Med* 2001, **28**, 136–143.
99. Rafecas M, Boning G, Pichler BJ, Lorenz E, Schwaiger M, Zeigler SI. Characterization and processing of inter-crystal scatter in a dual layer, high resolution LSO-APD-PET. In IEEE, ed. *IEEE Nucl. Sci. Symp Med Imag Conf*. San Diego, CA, 2001.
100. Cutler PD, Cherry S, Hoffman E, Digby WM, Phelps ME. Design features and performance of a PET system for animal research. *J Nucl Med* 1992, **33**, 595–604.
101. Watanabe M, Uchida H, Okada H, *et al*. A high resolution PET for animal imaging. *IEEE Trans Med Imag* 1992, **11**, 577–580.
102. Watanabe M, Okada H, Shimizu K, *et al*. A high resolution animal PET scanner using compact PS-PMT detectors. *IEEE Trans Nucl Sci* 1997, **44**, 1277–1282.
103. Bloomfield PM, Rajeswaran S, Spinks TJ, *et al*. The design and physical characteristics of a small animal positron emission tomograph. *Phys Med Biol* 1995, **40**, 1105–1206.
104. Bloomfield PM, Myers R, Hume SP, Spinks TJ, Lammertsma AA, Jones T. Three-dimensional performance of a small-diameter positron emission tomograph. *Phys Med Biol* 1997, **42**, 389–400.
105. Chatziioannou AF, Tai YC, Doshi N, Cherry SR. Detector development for microPET II: a 1 μl resolution PET scanner for small animal imaging. *Phys Med Biol* 2001, **46**, 2899–2910.
106. Shao Y, Silverman RW, Cherry SR, MacLaren DC. PET imaging of transgene expression. *Med Phys* 2000, **27**, 1535–1543.
107. Gambhir SS, Herschman HR, Cherry SR, *et al*. Imaging transgene expression with radionuclide imaging technologies. *Neoplasia* 2000, **2**, 118–138.
108. Gambhir SS, Barrio JR, Hershman HR, Phelps ME. Imaging gene expression: principles and assays. *J Nucl Cardiol* 1999, **6**, 219–233.
109. Gambhir SS, Barrio JR, Hershman HR, Phelps ME. Assays for noninvasive imaging of reporter gene expression. *Nucl Med Biol* 1999, **26**, 481–490.
110. Yaghoubi SS, Wu L, Liang Q, *et al*. Direct correlation between positron emission tomographic images of two reporter genes delivered by two distinct adenoviral vectors. *Gene Ther* 2001, **8**, 1072–1080.
111. Iyer M, Barrio JR, Namavari M, *et al*. 8-[^{18}F]Fluoropenciclovir: an improved reporter probe for imaging HSV1-tk reporter gene expression in vivo using PET. *J Nucl Med* 2001, **42**, 96–105.
112. Gambhir SS, Bauer E, Black ME, *et al*. A mutant herpes simplex virus type 1 thymidine kinase reporter gene shows improved sensitivity for imaging reporter gene expression with positron emission tomography. *Proc Natl Acad Sci* 2000, **97**, 2785–2790.
113. Gambhir SS, Barrio JR, Phelps ME, *et al*. Imaging adenoviral-directed reporter gene expression in living animals with positron emission tomography. *Proc Natl Acad Sci USA* 1999, **96**, 2333–2338.
114. Dehdashti F, Mortimer JE, Siegel BA, *et al*. Positron tomographic assessment of estrogen receptors in breast cancer: comparison with FDG-PET and in vitro receptor assays. *J Nucl Med* 1995, **36**, 1766–1774.
115. Mortimer JE, Dehdashti F, Siegel BA, Katzenellenbogen JA, Fracasso P, Welch MJ. Positron emission tomography with 2-[^{18}F]fluoro-2-deoxy-D-glucose and 16a-[^{18}F]-fluoro-17β-estradiol in breast cancer: correlation with estrogen receptor status and response to systemic therapy. *Clin Cancer Res* 1996, **2**, 933–939.
116. Oyama N, Jones LA, Sharp TL, Welch MJ. Androgenic control of glucose and acetate metabolism in rat prostate and prostate cancer tumour model. *Nucl Med* 2001, **42**, 26P.
117. Volkert WA, Hoffman TJ. Therapeutic radiopharmaceuticals. *Chem Rev* 1999, **99**, 2269–2292.
118. Katzenellenbogen JA, Coleman RE, Hawkins RA, *et al*. Tumor receptor imaging: proceedings of the National Cancer Institute Workshop, review of current work, and prospective for further investigations. *Clin Cancer Res* 1995, **1**, 921–932.
119. Cutler CS, Lewis JS, Anderson CJ. Utilization of metabolic, transport and receptor-mediated processes to deliver agents for cancer diagnosis. *Adv Drug Dev Rev* 1999, **37**, 189–211.
120. Reichert DA, Lewis JS, Anderson CJ. Metal complexes as diagnostic tools. *Coord Chem Rev* 1999, **184**, 3–66.
121. Goldenberg DM. *Cancer Imaging and Therapy with Radiolabeled Antibodies*. New York, Plenum Press, 1991.
122. Wu AM, Yazaki PJ, Tsai S, *et al*. High-resolution microPET imaging of carcinoembryonic antigen-positive xenografts by using a copper-64-labeled engineered antibody fragment. *Proc Natl Acad Sci USA* 2000, **97**, 8495–8500.
123. de Jong M, Breeman WAP, Bakker WH, *et al*. Comparison of 111In-labeled somatostatin analogues for tumor scintigraphy and radionuclide therapy. *Cancer Res* 1998, **58**, 437–441.
124. de Jong M, Bakker WH, Breeman WAP, *et al*. Preclinical comparison of [DTPA^{o}]octreotide, [DTPA^{o},Tyr^{3}]-octreotide and [DOTA^{o},Tyr^{3}]octreotide as carriers for somatostatin receptor-targeted scintigraphy and radionuclide therapy. *Int J Cancer* 1998, **75**, 406–411.
125. Lewis JS, Lewis MR, Srinivasan A, Schmidt MA, Wang J, Anderson CJ. Comparison of four ^{64}Cu-labeled somatostatin analogues *in vitro* and in a tumor-bearing rat model: evaluation of new derivatives for positron emission tomography imaging and targeted radiotherapy. *J Med Chem* 1999, **42**, 1341–1347.
126. Li WP, Lewis JS, Kim JY, *et al*. DOTA-D-Tyr^{1}-octreotate: a somatostatin analog for labeling with metal and halogen radiolnuclides for cancer imaging and therapy. *Bioconj Chem* 2002, **13**, 721–728.
127. Uger O, Kothari PJ, Finn RD, *et al*. Ga-66 labeled somatostatin analogue DOTA-DPhe^{1}-Tyr^{3}-octreotide as a potential agent for positron emission tomography imaging and receptor mediated internal radiotherapy of somatostatin receptor positive tumors. *Nucl Med Biol* 2002, **29**, 147–157.
128. Adonai N, Nguyen KN, Walsh J, *et al*. Ex vivo cell labeling with ^{64}Cu-pyruvaldehyde-bis(N^{4}-methylthiosemicarbazone) for imaging cell trafficking in mice with positron-emission tomography. *Proc Natl Acad Sci USA* 2002, **99**, 3030–3035.
129. Sun X, Kim YJ, Bigott B, Kovacs Z, Sherry AD, Welch MJ, Anderson CJ. A potential bone-imaging agent: copper-64-labeled 1,4,7,10-tetraazacyclododecane-1,4,7-*tri*(methanephosphonic acid) *J Nucl Med* 2002, **43**, 136P.

130. Shah N, Cerussi A, Eker C, *et al*. Noninvasive functional optical spectroscopy of human breast tissue. *Proc Natl Acad Sci USA* 2001, **98**, 4420–4425.
131. Hawrysz DJ, Sevick-Muraca EM. Developments toward diagnostic breast cancer imaging using near-infrared optical measurements and fluorescent contrast agents. *Neoplasia* 2000, **2**, 388–417.
132. Schotland JC. Continuous-wave diffusion imaging. *J Opt Soc Am A—Optics Image Sci Vision* 1997, **14**, 275–279.
133. Lee J, Sevick-Muraca E. Fluorescence-enhanced absorption imaging using frequency-domain photon migration: tolerance to measurement error. *J Biomed Opt* 2001, **6**, 58–67.
134. Cheong WF, vanHouten JP, Kermit EL, Machold TR, Stevenson DK, Benaron DA. Pilot comparison of light-based optical tomography versus ultrasound for real-time imaging of neonatal intraventricular hemorrhage. *Pediatric Res* 1996, **39**, 1189.
135. Rhine WD, Benaron DA, Darceuil HE, *et al*. Simultaneous time of-flight adjusted (TOFA) near-infrared spectroscopy and magnetic resonance imaging of immature rabbit hypoxic-ischemic encephalopathy (HIE). *Pediatric Res* 1996, **39**, 2264.
136. Wagnieres GA, Star WM, Wilson BC. In vivo fluorescence spectroscopy and imaging for oncological applications. *Photochem Photobiol* 1998, **68**, 603–632.
137. Ntziachristos V, Yodh AG, Schnall M, Chance B. Concurrent MRI and diffuse optical tomography of breast after indocyanine green enhancement. *Proc Natl Acad Sci USA* 2000, **97**, 2767–2772.
138. Cubeddu R, Pifferi A, Taroni P, *et al*. Fluorescence imaging during photodynamic therapy of experimental tumors in mice sensitized with disulfonated aluminum phthalocyanine. *Photochem Photobiol* 2000, **72**, 690–695.
139. Achilefu S, Dorshow RB, Bugaj JE, Rajagopalan R. Novel receptor-targeted fluorescent contrast agents for in vivo tumor imaging. *Invest Radiol* 2000, **35**, 479–485.
140. Bugaj JE, Achilefu S, Dorshow RB, Rajagopalan R. Novel fluorescent contrast agents for optical imaging of in vivo tumors based on a receptor-targeted dye-peptide conjugate platform. *J Biomed Opt* 2001, **6**, 122–133.
141. Bigio IJ, Mourant JR. Ultraviolet and visible spectroscopies for tissue diagnostics: fluorescence spectroscopy and elastic-scattering spectroscopy. *Phys Med Biol* 1997, **42**, 803–814.
142. Round AJ, Duller AWG, Fish PJ. Lesion classification using skin patterning. *Skin Res Tech* 2000, **6**, 183–192.
143. Wallace VP, Bamber JC, Crawford DC, Ott RJ, Mortimer PS. Classification of reflectance spectra from pigmented skin lesions, a comparison of multivariate discriminant analysis and artificial neural networks. *Phys Med Biol* 2000, **45**, 2859–2871.
144. So PTC, Kim H, Kochevar IE. Two-photon deep tissue ex vivo imaging of mouse dermal and subcutaneous structures. *Optics Express* 1998, **3**, 339–350.
145. Sterenborg H, Motamedi M, Wagner RF, Duvic M, Thomsen S, Jacques SL. In-vivo fluorescence spectroscopy and imaging of human skin tumors. *Lasers Med Sci* 1994, **9**, 191–201.
146. Villringer A, Chance B. Non-invasive optical spectroscopy and imaging of human brain function. *Trends Neurosci* 1997, **20**, 435–442.
147. Seville M. A whole new way of looking at things: the use of Dark Reader technology to detect fluorophors. *Electrophoresis* 2001, **22**, 814–828.
148. Tromberg BJ, Shah N, Lanning R, *et al*. Non-invasive in vivo characterization of breast tumors using photon migration spectroscopy. *Neoplasia* 2000, **2**, 26–40.
149. Brancaleon L, Durkin AJ, Tu JH, Menaker G, Fallon JD, Kollias N. In vivo fluorescence spectroscopy of nonmelanoma skin cancer. *Photochem Photobiol* 2001, **73**, 178–183.
150. Young AR. Chromophores in human skin. *Phys Med Biol* 1997, **42**, 789–802.
151. Reynolds JS, Troy TL, Mayer RH, *et al*. Imaging of spontaneous canine mammary tumors using fluorescent contrast agents. *Photochem Photobiol* 1999, **70**, 87–94.
152. Nioka S, Yung Y, Shnall M, *et al*. Optical imaging of breast tumor by means of continuous waves. *Adv Exp Med Biol* 1997, **411**, 227–232.
153. Sevick-Muraca EM, Lopez G, Reynolds JS, Troy TL, Hutchinson CL. Fluorescence and absorption contrast mechanisms for biomedical optical imaging using frequency-domain techniques. *Photochem Photobiol* 1997, **66**, 55–64.
154. Licha K, Riefke B, Ntziachristos V, Becker A, Chance B, Semmler W. Hydrophilic cyanine dyes as contrast agents for near-infrared tumor imaging: synthesis, photophysical properties and spectroscopic in vivo characterization. *Photochem Photobiol* 2000, **72**, 392–398.
155. Ntziachristos V, Chance B. Probing physiology and molecular function using optical imaging: applications to breast cancer. *Breast Cancer Res* 2001, **3**, 41–46.
156. Pelegrin A, Folli S, Buchegger F, Mach JP, Wagnieres G, Vandenbergh H. Antibody fluorescein conjugates for photoimmunodiagnosis of human colon-carcinoma in nude-mice. *Cancer* 1991, **67**, 2529–2537.
157. Vogel CA, Galmiche MC, Westermann P, *et al*. Carcinoembryonic antigen expression, antibody localisation and immunophotodetection of human colon cancer liver metastases in nude mice: a model for radioimmunotherapy. *Int J Cancer* 1996, **67**, 294–302.
158. Ballou B, Fisher GW, Hakala TR, Farkas DL. Tumor detection and visualization using cyanine fluorochrome-labeled antibodies. *Biotechnol Prog* 1997, **13**, 649–658.
159. Clauss MA, Jain RK. Interstitial transport of rabbit and sheep antibodies in normal and neoplastic tissues. *Cancer Res* 1990, **50**, 3487–3492.
160. Folli S, Westermann P, Braichotte D, *et al*. Antibody-indocyanin conjugates for immunophotodetection of human squamous-cell carcinoma in nude-mice. *Cancer Res* 1994, **54**, 2643–2649.
161. Ballou B, Fisher GW, Deng JS, Hakala TR, Srivastava M, Farkas DL. Cyanine fluorochrome-labeled antibodies in vivo: assessment of tumor imaging using Cy3, Cy5, Cy5.5, and Cy7. *Cancer Detect Prev* 1998, **22**, 251–257.
162. Ballou B, Fisher GW, Waggoner AS, *et al*. Tumor labeling in-vivo using cyanine-conjugated monoclonal-antibodies. *Cancer Immunol Immunother* 1995, **41**, 257–263.
163. Becker A, Hessenius C, Licha K, *et al*. Receptor-targeted optical imaging of tumors with near-infrared fluorescent ligands. *Nature Biotechnol* 2001, **19**, 327–331.
164. Stolz B, Weckbecker G, Smith-Jones PM, Albert R, Raulf F, Bruns C. The somatostatin receptor-targeted radiotherapeutic [Y-90-DOTA- DPhe(1),Tyr(3)]octreotide (Y-90-SMT 487) eradicates experimental rat pancreatic CA 20948 tumours. *Eur J Nucl Med* 1998, **25**, 668–674.
165. Urizzi P, Allen CM, Langlois R, Ouellet R, La Madeleine C, Van Lier JE. Low-density lipoprotein-bound aluminum sulfophthalocyanine: targeting tumor cells for photodynamic therapy. *J Porphyrins Phthalocyanines* 2001, **5**, 154–160.
166. Callahan DE, Forte TM, Afzal SMJ, *et al*. Boronated protoporphyrin (BOPP): localization in lysosomes of the human glioma cell line SF-767 with uptake modulated by lipoprotein levels. *Int J Radiat Oncol Biol Phys* 1999, **45**, 761–771.
167. Schmidt-Erfurth U, Diddens H, Birngruber R, Hasan T. Photodynamic targeting of human retinoblastoma cells using covalent low-density lipoprotein conjugates. *Br J Cancer* 1997, **75**, 54–61.
168. Maziere JC, Morliere P, Biade S, Santus R. Photochemotherapy of tumors—biochemical basis, therapeutic application and prospects. *Comptes Rendus Des Seances De La Societe De Biologie Et De Ses Filiales* 1992, **186**, 88–106.

169. Hamblin MR, Newman EL. Photosensitized targeting in photodynamic therapy 2. Conjugates of hematoporphyrin with serum-lipoproteins. *J Photochem Photobiol B-Biol* 1994, **26**, 147–157.
170. Allison BA, Pritchard PH, Levy JG. Evidence for low-density-lipoprotein receptor-mediated uptake of benzoporphyrin derivative. *Br J Cancer* 1994, **69**, 833–839.
171. Desmidt PC, Versluis AJ, Vanberkel TJC. Properties of incorporation, redistribution, and integrity of porphyrin low-density-lipoprotein complexes. *Biochemistry* 1993, **32**, 2916–2922.
172. Maziere JC, Morliere P, Santus R. New trends in photobiology (invited teview)—the role of the low-density-lipoprotein receptor pathway in the delivery of lipophilic photosensitizers in the photodynamic therapy of tumors. *J Photochem Photobiol B-Biol* 1991, **8**, 351–360.
173. Fischer F, Dickson EF, Kennedy JC, Pottier RH. An affordable, portable fluorescence imaging device for skin lesion detection using a dual wavelength approach for image contrast enhancement and aminolaevulinic acid-induced protoporphyrin IX. Part II. In vivo testing. *Lasers Med Sci* 2001, **16**, 207–212.
174. Hillemanns P, Weingandt H, Baumgartner R, Diebold J, Xiang W, Stepp H. Photodetection of cervical intraepithelial neoplasia using 5-aminolevulinic acid-induced porphyrin fluorescence. *Cancer* 2000, **88**, 2275–2282.
175. Hewett J, Nadeau V, Ferguson J, *et al*. The application of a compact multispectral imaging system with integrated excitation source to in vivo monitoring of fluorescence during topical photodynamic therapy of superficial skin cancers. *Photochem Photobiol* 2001, **73**, 278–282.
176. Subbarayan M, Shetty SJ, Srivastava TS, Noronha OPD, Samuel AM, Mukhtar H. Water-soluble Tc-99m-labeled dendritic novel porphyrins tumor imaging and diagnosis. *Biochem Biophys Res Commun* 2001, **281**, 32–36.
177. Hayase M, Woodbum KW, Perlroth J, *et al*. Photoangioplasty with local motexafin lutetium delivery reduces macrophages in a rabbit post-balloon injury model. *Cardiovasc Res* 2001, **49**, 449–455.
178. Lam S, MacAulay C, leRiche JC, Palcic B. Detection and localization of early lung cancer by fluorescence bronchoscopy. *Cancer* 2000, **89**, 2468–2473.
179. Sutton JM, Fernandez N, Boyle RW. Functionalized diphenylchlorins and bacteriochlorins: their synthesis and bioconjugation for targeted photodynamic therapy and tumour cell imaging. *J Porphyrins Phthalocyanines* 2000, **4**, 655–658.
180. van den Akker J, de Bruijn HS, van Henegouwen G, Star WM, Sterenborg H. Protoporphyrin IX fluorescence kinetics and localization after topical application of ALA pentyl ester and ALA on hairless mouse skin with UVB-induced early skin cancer. *Photochem Photobiol* 2000, **72**, 399–406.
181. Gurfinkel M, Thompson AB, Ralston W, *et al*. Pharmacokinetics of ICG and HPPH-car for the detection of normal and tumor tissue using fluorescence, near-infrared reflectance imaging: a case study. *Photochem Photobiol* 2000, **72**, 94–102.
182. Weissleder R, Tung CH, Mahmood U, Bogdanov A. In vivo imaging of tumors with protease-activated near-infrared fluorescent probes. *Nature Biotech* 1999, **17**, 375–378.
183. Bremer C, Tung CH, Weissleder R. In vivo molecular target assessment of matrix metalloproteinase inhibition. *Nature Med* 2001, **7**, 743–748.
184. Hoffman RM. Visualization of GFP-expressing tumors and metastasis in vivo. *Biotechniques* 2001, **30**, 1016–1022.
185. Yang M, Baranov E, Li XM, *et al*. Whole-body and intravital optical imaging of angiogenesis in orthotopically implanted tumors. *Proc Natl Acad Sci USA* 2001, **98**, 2616–2621.
186. Mahmood U, Tung CH, Bogdanov A, Weissleder R. Near-infrared optical imaging of protease activity for tumor detection. *Radiology* 1999, **213**, 866–870.
187. Moore A, Marecos E, Simonova M, Weissleder R, Bogdanov A. Novel gliosarcoma cell line expressing green fluorescent protein: a model for quantitative assessment of angiogenesis. *Microvascular Res* 1998, **56**, 145–153.
188. Edinger M, Sweeney TJ, Tucker AA, Adesuwa OB, Negrin RS, Contag CH. Noninvasive assessment of tumor cell proliferation in animal models. *Neoplasia* 1999, **1**, 303–310.
189. Becker A, Riefke B, Ebert B, *et al*. Macromolecular contrast agents for optical imaging of tumors: comparison of indotricarbocyanine-labeled human serum albumin and transferrin. *Photochem Photobiol* 2000, **72**, 234–241.